Downloaded from UvA-DARE, the institutional repository of the University of Amsterdam (UvA)
http://hdl.handle.net/11245/2.19179

File ID uvapub:19179
Filename 101017y.pdf
Version unknown

SOURCE (OR PART OF THE FOLLOWING SOURCE):
Type article
Title Measurements of the Magnetic Field Geometry and Strength in Bok Globules.
Author(s) T. Henning, S. Wolf, R. Launhardt, L.B.F.M. Waters
Faculty FNWI: Astronomical Institute Anton Pannekoek (IAP)
Year 2001

FULL BIBLIOGRAPHIC DETAILS:
http://hdl.handle.net/11245/1.194407

Copyright

It is not permitted to download or to forward/distribute the text or part of it without the consent of the author(s) and/or copyright holder(s), other than for strictly personal, individual use, unless the work is under an open content licence (like Creative Commons).

UvA-DARE is a service provided by the library of the University of Amsterdam (http://dare.uva.nl)
(pagedate: 2014-11-15)

THE ASTROPHYSICAL JOURNAL, 561:871–879, 2001 November 10
© 2001. The American Astronomical Society. All rights reserved. Printed in U.S.A.

MEASUREMENTS OF THE MAGNETIC FIELD GEOMETRY AND STRENGTH IN BOK GLOBULES

TH. HENNING
Astrophysikalisches Institut und Universitäts-Sternwarte, Schillergässchen 2-3, D-07745 Jena, Germany; henning@astro.uni-jena.de
S. WOLF
Thüringer Landessternwarte Tautenburg, Sternwarte 5, D-07778 Tautenburg, Germany; wolf@tls-tautenburg.de
R. LAUNHARDT
Division of Physics, Mathematics and Astronomy, California Institute of Technology, MS 105-24, Pasadena, CA 91125; rl@astro.caltech.edu
AND
R. WATERS
Astronomical Institute, University of Amsterdam, Kruislaan 403, 1098 SJ Amsterdam, Netherlands; rensw@astro.uva.nl
Received 2001 January 8; accepted 2001 July 18

ABSTRACT

In order to study the influence and structure of the magnetic field in the early phases of low-mass star formation, we obtained polarization maps of three Bok globules at a wavelength of 850 μm, using the Submillimeter Common-User Bolometer Array at the James Clerk Maxwell Telescope. We observed the following sources: CB 26, a globule with a nearly dispersed dense core containing a source with a circumstellar disk; CB 54, a deeply embedded young stellar cluster; and DC 253−1.6 (CG 30), a protostellar double core. We find strongly aligned polarization vectors in the case of CB 26 and DC 253−1.6, while the vector orientations in the case of CB 54 are more or less randomly distributed. The degree of polarization, amounting to several percent, was found to decrease toward the center in each source. In the case of CB 54 and DC 253−1.6, the degree of polarization similarly depends on the corresponding intensity. Assuming dichroic emission by aligned nonspherical grains as the polarization mechanism, where the magnetic field plays a role in the alignment process, we derive magnetic field strengths and structures from the observed polarization patterns. In the case of the double core DC 253−1.6, we discuss the correlation between the fragmentation process and the magnetic field direction.

Subject headings: ISM: clouds — ISM: individual (CB 26, CB 54, DC 253−1.6) — ISM: magnetic fields — techniques: polarimetric

On-line materials: color figures

1. INTRODUCTION

Magnetic fields are an important factor in the star formation process (see, e.g., Greaves et al. 1999; McKee 1999; Mouschovias & Ciolek 1999; Shu et al. 1999). They can influence the contraction timescale, the gas-dust coupling, and the shape of cloud fragments. In the dusty envelopes around young stellar objects (YSOs), polarization due to dichroic extinction and thermal emission by spinning dust grains is the most important signature of magnetic fields (see, e.g., Weintraub, Goodman, & Akeson 2000; Clemens & Kraemer 1999; Greaves, Murray, & Holland 1994). The dust grains become partially aligned with the magnetic field, generally with their long axes perpendicular to the field (see, e.g., Lazarian, Goodman, & Myers 1997; Draine & Weingartner 1997). Thus, the thermal emission from grains at far-infrared and millimeter wavelengths is partially linearly polarized, with a polarization direction perpendicular to the magnetic field as projected onto the plane of sky. From multiwavelength polarimetric measurements in combination with simultaneously obtained intensity maps, the magnetic field structure and strength, the dust density distribution, chemical composition, a rough estimate of the dust grain size and shape distribution, and the grain alignment rate can be derived (see, e.g., Goodman 1996). Such observations should allow an assessment of the relative importance of uniform and tangled fields. A high level of polarization, uniform in direction, indicates a well-ordered field that is not significantly tangled on scales smaller than the beam size.

Because of their relatively isolated location, Bok globules are well suited for studying the direct interplay between protostellar collapse, fragmentation, and magnetic fields since they are less affected by strong turbulence and other nearby star-forming events. The submillimeter continuum maps trace mainly the dense cores, which often consist of central condensations unresolved in single-dish observations and their envelopes. The central condensation can just represent the central dense and warm part of the protostellar core, or an embedded unresolved circumstellar disk (see the description of CB 26 in § 2). The observations are not sensitive to the low-density material along the path length between the observer and the Bok globule. Thus, one should be able to test the geometrical predictions of theoretical models for star-forming clouds.

Recently, first observations of the magnetic field geometry in three prestellar cores have been performed by Ward-Thompson et al. (2000). Davis et al. (2000) measured the polarization of the 850 μm dust continuum emission associated with class 0/I protostars in the Serpens dark cloud core. Furthermore, Matthews & Wilson (2000) concluded from polarimetric measurements of OMC-3 in Orion A that the magnetic field is predominantly perpendicular to the filament along most of its length. Earlier results of far-infrared and (sub)millimeter polarization observations have been summarized by Weintraub et al. (2000). With respect to the data analysis, we want to mention the work by Basu (2000) and Minchin, Bonifaćio, & Murray (1996) on the effect of the viewing angle on the

observed polarization position angles. These authors show that the projected direction of the magnetic field is often slightly misaligned with the projected minor axis of a molecular cloud core and/or the direction of a possible outflow.

In systematic 1.2 mm continuum and CS line surveys of nearly 100 Bok globules selected from the catalogs of Clemens & Barvainis (1988) and Hartley et al. (1986), we detected ~40 dense cores, most of which show signatures of star formation (Launhardt & Henning 1997; Launhardt et al. 1998; Henning & Launhardt 1998). Analyzing the optical properties, near-IR–to–millimeter spectral energy distributions, and the emission of high-density molecular tracers of a large number of globule cores, we were able to divide the objects into different evolutionary stages reaching from prestellar cores, through protostellar cores with spectroscopic signature of collapse, to disk-dominated objects. In two former James Clerk Maxwell Telescope (JCMT) observing runs, we measured 10/4 globule cores at 450 and 800 μm using UKT14/SCUBA (Launhardt, Ward-Thompson, & Henning 1997; R. Launhardt et al. 2001c, in preparation). For these cores, we also obtained 1.2 mm bolometer maps with the IRAM 30 m telescope (R. Launhardt, Th. Henning, & R. Zylka 2001d, in preparation). Here we present polarization maps at 850 μm of three well-characterized Bok globules.

In § 2 we summarize what is known about the sources. Our observations and data reduction are described in §§ 3 and 4. In § 5.2 we present the obtained polarization maps. Assuming dichroic emission by aligned nonspherical grains, where the magnetic field is important for the alignment, we derive the mean magnetic field strength in the three Bok globules in § 5.3. Furthermore, we consider the relation between the polarization and intensity distribution in § 5.4. Finally, we discuss the correlation between the fragmentation process and the magnetic field direction in the double-core system DC 253 − 1.6.

2. DESCRIPTION OF THE SOURCES

We observed the Bok globules CB 26, CB 54, and DC 253 − 1.6 (see Table 1).

CB 26 (L1439) is a small, slightly cometary-shaped Bok globule at $D \sim 140$ pc (Launhardt, Sargent, & Zinnecker 2001b; note that Launhardt & Henning 1997 used a distance of 300 pc). The globule contains a small bipolar near-infrared (NIR) nebula that is associated with strong submillimeter/millimeter continuum emission. The embedded star responsible for the reflection nebula is deeply embedded and not seen even at 2.2 μm. Follow-up observations with the Owens Valley millimeter interferometer revealed a large rotating disk at the submillimeter continuum peak position, which matches an extinction lane at the center of the NIR nebula. The disk orientation position angle amounts to 60°. This disk completely dominates the flux density of the unresolved component in the SCUBA map (Fig. 2). The dense, protostellar core is nearly dispersed, and a remnant envelope with $M_{\rm H} \sim 0.1\ M_\odot$ is seen in the 850 μm map. The spectral energy distribution together with the total luminosity of $L \sim 0.7\ L_\odot$ and the rotation curve of the circumstellar disk suggest the presence of a 0.3–0.5 $M_\odot$ class I YSO in CB 26 (Launhardt et al. 2001b).

CB 54 is a large Bok globule associated with the molecular cloud BBW 4 at $D \sim 1.1$ kpc (Brand & Blitz 1993) and the reflection nebula LBN 1042 (Lynds 1965). The globule contains a massive dense core of $M_{\rm H} \sim 100\ M_\odot$, which is associated with a bipolar molecular outflow with a position angle of 30° (Launhardt & Henning 1997; R. Launhardt et al. 2001d in preparation; Yun & Clemens 1994) and shows spectroscopic signatures of mass infall (Launhardt et al. 1998). Projected against the dense core is a small young stellar NIR cluster that was probably born in this large globule (Yun 1996; Launhardt 1996; R. Launhardt et al. 2001c, in preparation; see also Fig. 1). However, no NIR source is associated with the peak of the submillimeter continuum emission (R. Launhardt et al. 2001c, in preparation).

DC 253 − 1.6 (CG 30; Zealey et al. 1983; BHR 12; Bourke, Hyland, & Robinson 1995) is a bright-rimmed cometary globule located in the Gum Nebula region. It was generally assumed to be ~400 pc away, but new measurements suggest a distance of only 200 pc to the CG 30/31/38 complex (Knude, Jønch-Sørensen, & Nielsen 1999). The center of CG 30 contains the embedded infrared source IRS 4 and the associated Herbig-Haro nebula HH 120 (see Hodapp & Ladd 1995 and references therein). The globule has an elongated dense core of $M_{\rm H} \sim 3\ M_\odot$ as seen in the millimeter dust continuum emission (R. Launhardt et al. 2001c, in preparation). The SCUBA observations presented in this paper resolve this core into two subcores with a projected separation of 20″ (≃4000 AU at 200 pc) and masses of $\sim 0.17 \pm 0.05$ and $\sim 0.14 \pm 0.05\ M_\odot$ for the northern and southern subcores, respectively. The northern core is associated with an NIR nebula (IRS 4). The southern core is the origin of a protostellar jet with a position angle of 44° (Hodapp & Ladd 1995), but no NIR source is seen at the submillimeter continuum position (see Launhardt et al. 2001a). These two subcores are unresolved in the SCUBA beam, and the flux contribution from possible disks is

TABLE 1

COORDINATES, DISTANCES, AND FLUX DENSITIES OF THE OBSERVED GLOBULES

Object	Other Names[a]	IRAS Source	R.A.[b]	Decl.[b]	Distance (pc)	F_{450}[c] (Jy)	F_{850}[c] (Jy)
CB 26	L1439	04559+5200	04 55 54.6	+52 00 15	140	11 (3.2)	1.0 (0.47)
CB 54	LBN 1042	07020−1618	07 02 06.0	−16 18 51	1100	74 (9.3)	7.4 (1.5)
DC 253.3−1.6-N.....	BHR 12, HH 120	08076−3556	08 07 40.4	−35 56 06	200	30 (3.0)	7.4 (1.2)
DC 253.3−1.6-S	BHR 12, HH 120	08076−3556	08 07 40.1	−35 56 26		(3.7)	(1.0)

NOTE.—Units of right ascension are hours, minutes, and seconds, and units of declination are degrees, arcminutes, and arcseconds.

[a] L: Lynds 1962; LBN: Lynds 1965; BHR: Bourke et al. 1995.

[b] B1950 coordinates of the submillimeter peak(s).

[c] Total flux density integrated within a polygon around the closed 2 σ contour (value in parentheses is the peak flux density in janskys per beam).

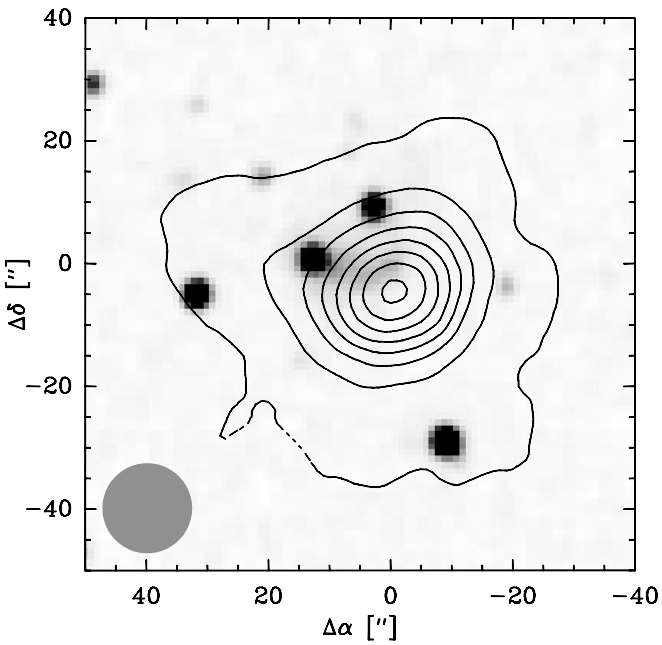

FIG. 1.—*K*-band image of CB 54 (gray-scale; 2MASS) overlaid with contours of the 850 μm dust continuum map. Contour levels are at 10%–97.5% with steps of 12.5% of the peak surface brightness 0.87 Jy beam^{-1}. The gray area represents the HPBW size of the 850 μm beam.

unknown. A detailed analysis of this source will follow in a separate paper. We are currently investigating whether this double core forms a bound protobinary system or not.

3. OBSERVATIONS

The observations were performed at the 15 m JCMT on Mauna Kea (Hawaii) between 2000 March 1 and 6. The effective beam sizes (HPBW) are $\sim$14.″7 at 850 μm and $\sim$8.″0 at 450 μm. The polarimetry was conducted using SCUBA (Holland et al. 1999) and its polarimeter, SCUPOL. The polarimeter consists of a combination of a rotating half-wave plate and a fixed analyzer that modulates the polarized signal with the orientation of the wave plate's optical axis (Greaves et al. 2000). We used the 350–850 μm achromatic half-wave plate in the current observations. More details of the polarimeter hardware can be found in Murray et al. (1997).

The SCUBA polarimeter can be used either as an imaging polarimeter or as a photopolarimeter. Our targets have a protostellar core/disk-envelope structure with envelope sizes smaller than 2′. Therefore, we used the imaging mode of SCUBA. Fully sampled 16 point jiggle maps have been obtained for each object, whereby each jiggle map was repeated 16 times with the wave plate stepped by 22.°5 between the individual maps. This mode allows imaging polarimetry with a 2.′3 field of view at the long (750/850 μm) and short (350/450 μm) wavelengths simultaneously. Although observations were made at 850 and 450 μm (simultaneously), only 850 μm data are presented in this paper because the signal-to-noise ratio was too low for the 450 μm data.

4. DATA REDUCTION

The data reduction package SURF (see Jenness & Lightfoot 1998) was used for flat-fielding, extinction correction, sky-noise removal (see Jenness, Lightfoot, & Holland 1998), and instrumental polarization removal. The Stokes parameters I, Q, and U were computed for each set of the 16 maps using the POLPACK data reduction package (Berry & Gledhill 1999) by averaging maps taken at the same wave plate orientation followed by fitting a sine wave to each image pixel. This set of Stokes parameters was then averaged and binned (over a 9″ region) before calculating the average degree of linear polarization P_l and position angle γ for each pixel.

Since the chop throw was 120″ (azimuth), the very outer regions in the jiggle maps (which are also undersampled) may suffer from chopping into the outermost envelope regions and into extended low-level emission from the thin outer regions of the globules. We therefore restrict the polarization analysis to the inner 60″ of the maps and do not use the outer $\sim$20″. We also restrict the polarization analysis to the regions in which the total flux density per beam is above 5 times the rms in the maps (measured outside the central sources). We did not use polarization vectors derived at positions where the scatter of the total flux density measurements between the jiggle cycles was larger than 20% of the average total flux density at that point. Furthermore, polarization vectors with $\sigma(P_l)/P_l < 3$, where $\sigma(P_l)$ is the standard deviation of the degree of polarization, have been excluded. These selection criteria ensure that only high-quality data are used for the polarization analysis and that the outer map regions, which may possibly be slightly affected by systematic effects from the chopping procedure, are avoided. We should note that the internal quality criteria of POLPACK already ensure that only significant polarization vectors are taken into account. This means that the maps with our strict quality criteria contain only about 20% fewer polarization vectors than the original maps.

5. RESULTS

5.1. *Masses and Densities*

In addition to the polarization maps, fully sampled nonpolarimetric jiggle maps of all three sources were obtained at both 450 and 850 μm. Beam maps and calibration factors were derived by observing five secondary calibrators (no planets were observed). The estimated calibration uncertainty is 30%. Peak flux densities (in janskys per beam; cf. § 3) and total flux densities integrated within a polygon around the closed 2 σ contour are compiled in Table 1.

All sources have unresolved compact condensations and envelopes with well-defined outer boundaries within the mapped areas. Condensation and envelope cannot be fitted by a single density profile. More extended low-level emission from the clouds is partially but not fully recovered. The uncertainty of the derived envelope flux densities introduced by this extended cloud emission is smaller than or comparable to the calibration uncertainty.

In order to derive masses and densities of the envelopes from the 850 μm maps, the compact condensations were modeled as Gaussian sources and subtracted from the maps. Since the structure of these compact sources is not resolved, they are not considered further here. Assuming isothermal emission, the density structure of the envelopes could be modeled by Gaussian profiles. Power-law profiles are inconsistent with the observed emission structure. FWHM sizes of the envelopes are in the range 60″–70″. The densities listed in Table 2 and used to calculate the magnetic

TABLE 2

MASSES, GAS DENSITIES, POLARIZATION, AND MAGNETIC FIELD STRENGTHS OF THE ENVELOPES

Object	$M_{\rm H}^{\rm enva}$ ($M_\odot$)	$\langle n_{\rm H}\rangle^{\rm b}$ (cm^{-3})	$\rho_{\rm Gas}$ (g cm^{-3})	$v_{\rm turb}$ (km s^{-1})	$N_{\rm vec}$	$\bar{\gamma}$ (deg)	$\sigma_{\bar{\gamma}}$ (deg)	B (μG)
CB 26	0.1	1.0E+5	2.3E−19	0.25[c]	7	25.3	$18.9^{+16.7}_{-7.3}$	74^{+47}_{-35}
CB 54	70	5.0E+4	1.1E−19	0.65[d]	41	−68.0	$42.7^{+11.1}_{-8.0}$	60^{+11}_{-8}
DC 253−1.6.....	2.1	2.5E+5	5.7E−19	0.25[c]	49	14.4	$38.2^{+8.9}_{-6.6}$	16^{+3}_{-3}

[a] Total envelope mass, derived from F_{850} after subtraction of the central unresolved condensation, assuming $T_d = 20$ K, $\kappa_{850} = 1.0$ cm^2 g^{-1}, and optically thin emission.

[b] Half-maximum value of a Gaussian density model profile fitted to the ring-averaged 850 μm emission profile (FWHM sizes 60″–70″).

[c] No direct value available; rms turbulence velocity of a large sample of nearby star-forming Bok globules derived from $C^{18}O$ ($J = 2$–1).

[d] Wang et al. 1995.

field strengths are half-maximum values of Gaussian density profile fits to the envelopes, derived with $T_d = 25$ K, $\kappa_{850} = 1.0$ cm^2 per gram of dust, and $M_{\rm H}/M_d = 100$. To account for helium and heavy elements, we derive the total gas density $\rho_{\rm Gas}$ from the atomic hydrogen density $n_{\rm H}$ (see Table 2) by

$$\rho_{\rm Gas} = 1.36 n_{\rm H} M_{\rm H} , \quad (1)$$

where $M_{\rm H} = 1.00797$ amu is the mass of a hydrogen atom.

5.2. *Polarization Maps*

The polarization maps of the Bok globules CB 26, CB 54, and DC 253−1.6 at 850 μm are shown in Figures 2, 3, and 4. Here we should remind the reader that we measure the polarization of radiation emitted by dust grains. Therefore, the lower degree of polarization in the cores cannot be the result of "depolarization" of polarized background radiation. For a more detailed discussion of this behavior, we refer to § 5.4.

In Figure 5 we plot the polarization histogram for each globule. Taking into account that the distributions $N(P_l)$

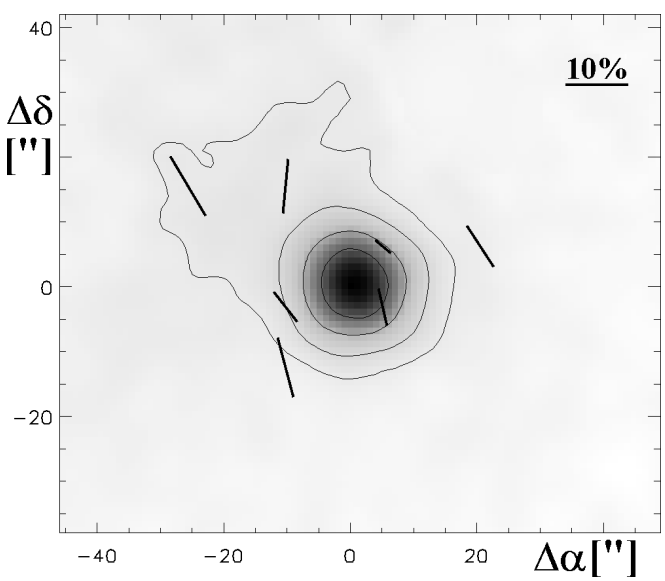

FIG. 2.—SCUBA 850 μm map of CB 26 with polarization vectors superposed. The length of the vectors stands for the degree of polarization, and the direction gives the position angle. The data are binned over 9″. Only vectors in which the 850 μm flux exceeds 5 times the standard deviation and $P_l/\sigma(P_l) > 3$ are plotted. The contour lines mark the levels of 10%, 25%, 50%, and 75% of the maximum intensity.

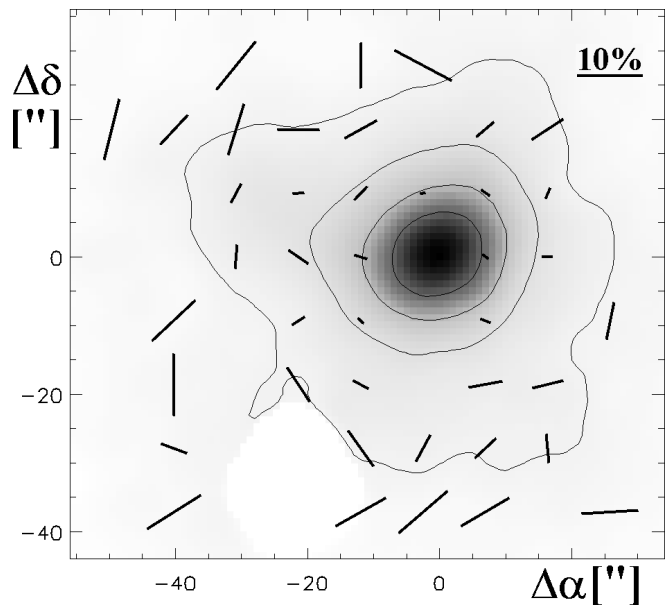

FIG. 3.—Same as Fig. 2 but for CB 54. The white area is caused by an incomplete coverage of the field.

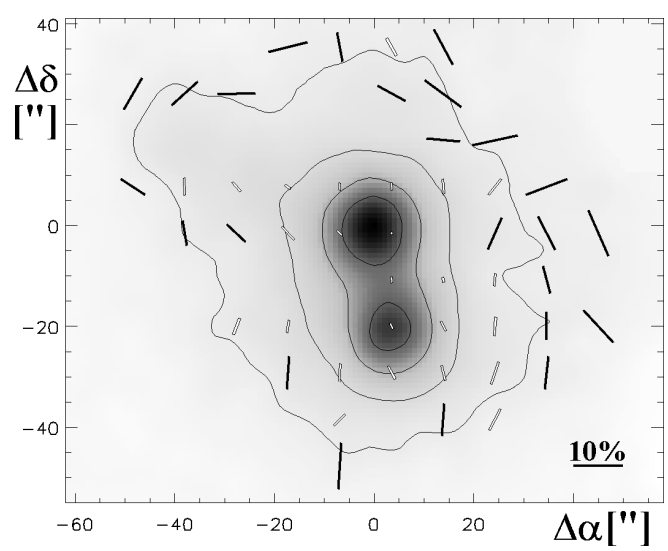

FIG. 4.—Same as Fig. 2 but for DC 253−1.6. The white vectors represent degrees of polarization smaller than 5% (see also Fig. 8).

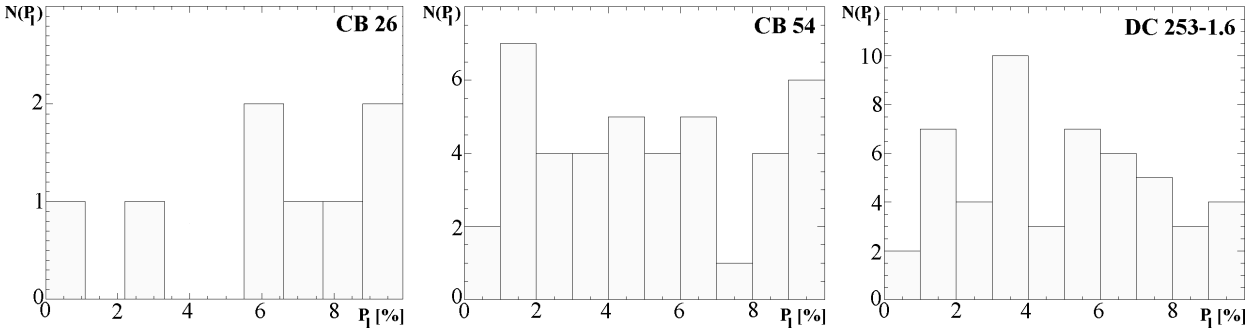

FIG. 5.—Histograms showing the distribution of the degree of polarization around CB 26, CB 54, and DC 253−1.6. [*See the electronic edition of the Journal for a color version of this figure.*]

are strongly influenced by statistical noise because of the small number of data points, we find an equipartition of degrees of polarization in the considered range $P_l =$ 0%–10%. The mean percentages of degrees of polarization for CB 26, CB 54, and DC 253−1.6 are 7.3%, 5.1%, and 5.0%. The corresponding 1 σ dispersions are 2.5%, 2.9%, and 2.6%.

For an unequivocal and profound interpretation of polarization maps, it is essential to determine the prevailing polarization mechanisms. Scattering by grains, which has often been taken into account for the interpretation of visible/NIR polarization maps of YSOs (see, e.g., Bastien & Ménard 1988; Fischer, Henning, & Yorke 1994), cannot produce the measured degrees of polarization because of the low albedo of dust grains at submillimeter wavelengths. In addition, the observed non-centrosymmetric polarization patterns would not be present if the illuminating source were surrounded by a nearly centrosymmetric dust density distribution, which can be assumed for CB 26 and CB 54. Thus, polarized thermal emission by aligned nonspherical grains remains as the main source of polarized submillimeter radiation in Bok globules (see, e.g., Weintraub et al. 2000; Greaves et al. 1999). This is similar to the situation in larger molecular clouds in which degrees of linear polarization up to 9% have been measured (see, e.g., Dowell 1997; Novak et al. 1997; Hildebrand 1996; Hildebrand et al. 1990, 1993; Morris et al. 1992; Gonatas et al. 1990) and interpreted to be caused by dichroic emission from aligned spheroidal dust grains (see, e.g., Greaves et al. 1999; Efstathiou, McCall, & Hough 1997; Wood 1996, 1997; Larson, Whittet, & Hough 1996; Casali 1995; Hildebrand & Dragovan 1995; Whittet et al. 1994).

5.3. *Magnetic Fields*

Nonspherical dust grains are expected to be aligned by the following mechanisms: paramagnetic relaxation (Davis & Greenstein 1951; Purcell 1975, 1979), supersonic flows (Gold 1951; Lazarian 1995), and/or radiative torques (Draine & Weingartner 1996, 1997). As has been shown by Lazarian et al. (1997) in the case of the filamentary dark cloud L1755, the Davis-Greenstein alignment mechanism is not expected to play an important role since the gas and dust have the same temperature. Furthermore, we have no evidence for strong supersonic flows in our objects. Draine & Weingartner (1997) pointed out that radiative torques on irregular dust grains, in addition to producing superthermal rotation, play a direct dynamical role in the alignment of dust grains with the local magnetic field. Such radiative torques can be important either in the outer regions of molecular clouds or in massive star-forming regions.

Irrespective of the alignment mechanism, charged interstellar grains would have a substantial magnetic moment, leading to a rapid precession of the grain angular momentum $\boldsymbol{J}$ around the magnetic field direction $\boldsymbol{B}$ (see Draine & Weingartner 1997 and references therein). This implies a net alignment of the grains with the magnetic field.

Based on the work by Chandrasekhar & Fermi (1953), the dispersion of polarization position angles is thought to be inversely proportional to the magnetic field strength. Thus, a uniform polarization pattern implies a uniform and strong magnetic field. The projected magnetic field vectors are oriented perpendicular to the direction of the polarization observed.

An estimate of the magnetic field strength (in units of gauss) can be derived from the polarization maps as follows (see Chandrasekhar & Fermi 1953):

$$B = |\boldsymbol{B}| = \sqrt{\frac{4\pi}{3}\,\rho_{\rm Gas}}\,\frac{v_{\rm turb}}{\sigma_{\bar{\gamma}}}\,. \tag{2}$$

Here $\rho_{\rm Gas}$ is the gas density (in units of g cm^{-3}), $v_{\rm turb}$ the rms turbulence velocity (in units of cm s^{-1}), and $\sigma_{\bar{\gamma}}$ the standard deviation to the mean orientation angle $\bar{\gamma}$ of the polarization vectors (in units of radians). This angle is given by

$$\bar{\gamma} = \frac{1}{2}\arctan\left(\frac{\sum_{i=1}^{N_{\rm vec}} U_i}{\sum_{i=1}^{N_{\rm vec}} Q_i}\right). \tag{3}$$

Here $N_{\rm vec}$ is the number of polarization vectors fulfilling the three criteria given in § 4, and Q and U are the Stokes vector components. Thus, the angle $\bar{\gamma}$ represents the orientation of the net polarization of the source. This treatment is based on the assumption that the magnetic field is frozen in the cloud material. Equation (2) agrees quite well with the relation by Crutcher (1999), who found that the magnetic field strengths scale with gas densities as

$$B \propto \rho_{\rm Gas}^{\kappa}\,, \tag{4}$$

where $\kappa \approx 0.47$. This also agrees with the prediction of ambipolar diffusion–driven star formation (Fiedler & Mouschovias 1993). We want to mention that Ostriker, Stone, & Gammie (2001) found, from the results of three-dimensional numerical magnetohydrodynamical simulations of giant molecular clouds, that equation (2) should be slightly modified by a factor of $\approx$0.88, provided $\sigma_{\bar{\gamma}} \leq 25°$ (see also Padoan et al. 2001 and references therein). Here we should note that the Chandrasekhar-Fermi formula is not

expected to hold for large dispersions of polarization angles. However, investigations by Padoan et al. (2001) indicate that the Chandrasekhar-Fermi formula may even be applied in this case if an appropriate correction factor is used.

We cannot exclude substructures of the dust configurations (and magnetic fields) on scales smaller than the beam size of our single-dish observations. Thus, the polarization measurements present an average over the small-scale magnetic field structure. Furthermore, as outlined by Zweibel (1990), in an inhomogeneous medium, ambipolar diffusion allows field lines to slip out of clumps, leading to straighter lines, a more ordered polarization pattern, and consequently a further overestimate of the field strength by a factor of up to 1.5. The magnetic field strengths, derived for CB 26, CB 54, and DC 253−1.6, are therefore upper limits.

The histograms of the orientation angle and the resulting standard deviations $\sigma_{\bar{\gamma}}$ are shown in Figure 6 and compiled in Table 2. In the case of CB 26, we find the clearest alignment of the polarization vectors ($\bar{\gamma} = 25\overset{\circ}{.}3$, $\sigma_{\bar{\gamma}} = 18\overset{\circ}{.}9$). However, a statistical analysis is hardly possible because only seven polarization vectors fulfill the quality criteria.

The linear polarization measured in CB 54 shows orientations being equally distributed over the entire angular range (−90°–+90°). The standard deviation $\sigma_{\bar{\gamma}} = 42\overset{\circ}{.}7$ is therefore very close to the theoretical value of $\sigma_{\bar{\gamma},\mathrm{ED}} = (30\sqrt{3})^\circ$ that can be derived in the case of an ideal equipartition [$N(\gamma) = \mathrm{const.}$]. Here one has to take into account that the mapped region is larger by a factor of 4–5 than that of CB 26 and DC 253−1.6. Because of the larger distance of CB 54, we see the result of the interference of the interstellar magnetic field with the magnetic field of the globule and the resulting grain disalignment in the outermost low-density regions of its envelope, which is much more effective than in the inner regions of the envelopes of CB 26 and DC 253−1.6. In addition, we should note that CB 54 is associated with a rather massive and energetic molecular outflow that may influence the structure of the object.

In the case of DC 253−1.6, we find again an alignment of the polarization vectors ($\bar{\gamma} = 14\overset{\circ}{.}4$, $\sigma_{\bar{\gamma}} = 38\overset{\circ}{.}1$). Considering a subset of polarization vectors with degrees of polarization lower than 5%, we find that the distribution $N(\gamma)$ is even more narrow (see dark distribution in the histogram for DC 253−1.6 in Fig. 6), resulting in a decreased standard deviation of $\sigma_{\bar{\gamma}} = 27\overset{\circ}{.}9$. From Figure 6 we find that the small degrees of linear polarization are measured close to the two protostellar condensations while larger polarization values are found in the outer regions of the envelope (for further discussions of this behavior see § 5.4; see also Weintraub et al. 2000).

The resulting magnetic fields, determined by the application of equation (2), are $B_{\mathrm{CB\,26}} \approx 74$ μG, $B_{\mathrm{CB\,54}} \approx 60$ μG, and $B_{\mathrm{DC\,253}} \approx 16$ μG. The magnetic field strengths we derived are comparable to those found in molecular clouds (see, e.g., Bhatt & Jain 1992), pre-protostellar cores (Levin et al. 2001), and other star-forming regions (see, e.g., Davis et al. 2000; Glenn, Walker, & Young 1999; Itoh et al. 1999; Minchin & Murray 1994; Chrysostomou et al. 1994; Crutcher 1999). The error estimates for the value of the standard deviation of the mean orientation angle $\sigma_{\bar{\gamma}}$ are based on a χ^2 test assuming a standard Gaussian distribution of the orientations of the polarization vectors. The error intervals given in Table 2 are based on confidence intervals for $\sigma_{\bar{\gamma}}$. The probability for the real (unknown) $\sigma_{\bar{\gamma},\mathrm{real}}$ to be included in this interval amounts to 95%. Based on this error estimate for $\sigma_{\bar{\gamma}}$, we give error intervals for the magnetic field strength B.

One has also to take into account the possibility of a considerable variation of the magnetic field strength between the envelope and the central region. This assumption is supported by the result of Itoh et al. (1999), who found $B = 0.07 \pm 0.02$ mG in the lobes of DR 21, while Roberts, Dickel, & Goss (1997) found $B \sim 0.5$ mG at a position nearer to the H II core of this object.

5.4. P_l *versus* I *Behavior*

In the case of CB 54 and DC 253−1.6, the degree of polarization decreases toward regions of increasing intensity (see Fig. 7; in the case of CB 26 the number of polarization vectors matching the applied selection criteria is too low to perform any statistical analysis; see also Fig. 5). A correlation between the intensity I and the degree of linear polarization P_l has also been found in other star-forming cores (see, e.g., Minchin et al. 1996; Glenn et al. 1999), in the molecular cloud OMC-3 in Orion A by Matthews & Wilson (2000), and in the Serpens dark cloud core, which contains several class 0/I protostars (Davis et al. 2000; see also references in Weintraub et al. 2000). It can be explained by the following effects:

1. Because of increased densities in the brighter cores, the collisional disalignment rate of the grains increases toward the centers of the cores.

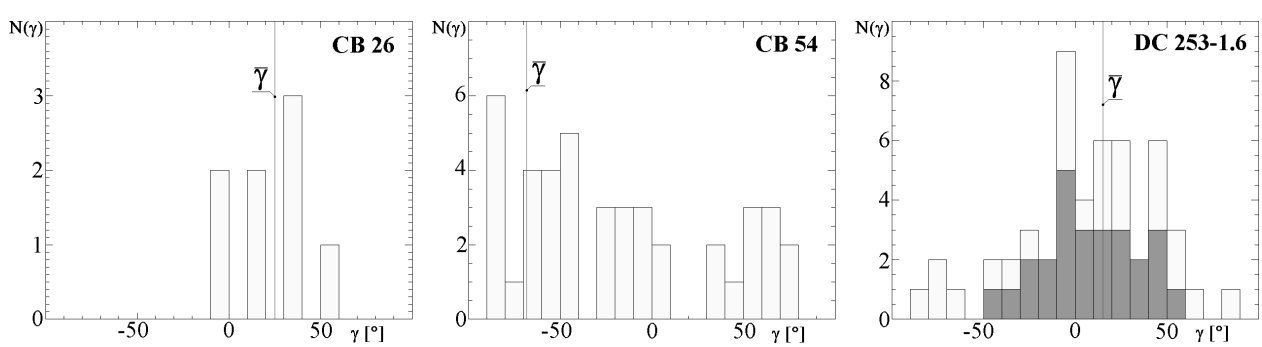

FIG. 6.—Histograms showing the distribution of position angles around CB 26, CB 54, and DC 253−1.6. Only data points in which the 850 μm flux exceeds 5 times the standard deviation and $P_l/\sigma(P_l) > 3$ have been considered. In the case of DC 253−1.6, the dark gray distribution represents the contribution of polarization vectors with $P_l < 5\%$ to the entire distribution. [*See the electronic edition of the Journal for a color version of this figure.*]

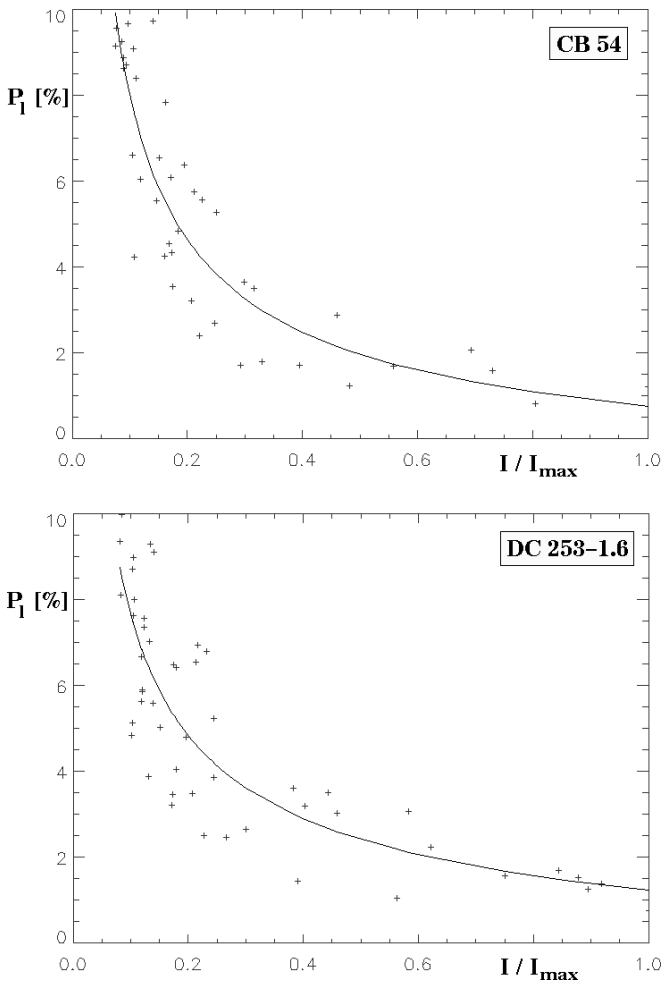

FIG. 7.—Scatter diagrams showing the distribution of P_l vs. intensity I across CB 54 and DC 253−1.6. Only data in which the 850 μm flux exceeds 5 times the standard deviation, $P_l/\sigma(P_l) > 3$, and $P_l < 10\%$ have been considered. Fits to the two sets of the data described by functions of the form $P_l = a_0 + a_1[I/\max(I)]^{a_2}$ are superposed on the data points (see § 5.4).

2. The field structure associated with the core collapse may be still unresolved in our polarization pattern (see, e.g., Shu, Adams, & Lizano 1987).

3. Spherical grain growth in the denser regions would result in unpolarized reemission by the dust (Weintraub et al. 2000).

A combination of the effects/explanations is possible. Because of the density gradient between the globule cores, particularly the large density contrast between the unresolved central condensations and the envelopes, we expect that increasingly poor grain alignment as density increases is the main effect. This hypothesis is similar to that offered for background starlight polarimetry in dark clouds (Goodman et al. 1992, 1995; Jones, Klebe, & Dickey 1992; Lazarian et al. 1997; Arce et al. 1998). However, we cannot rule out the other alternatives (see also Hildebrand et al. 1999).

Davis et al. (2000) applied linear least-square fits to the measured polarization as a function of the intensity and found a correlation between these quantities in two separated clusters of the Serpens cloud core. However, the decrease of the polarization toward increasing intensity measured in

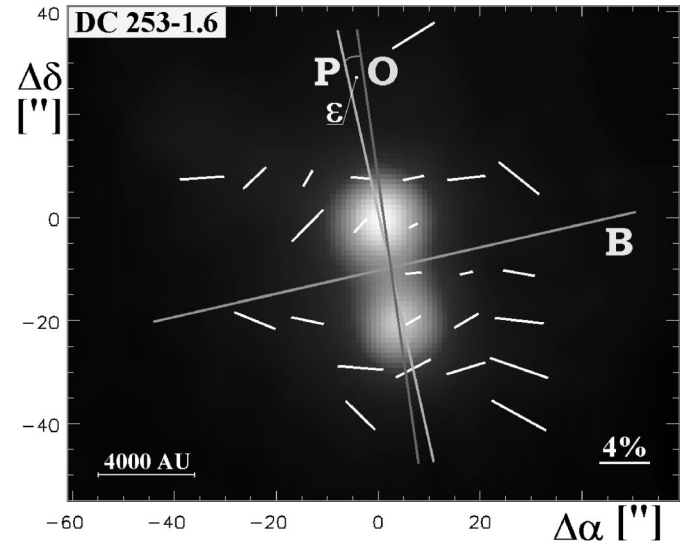

FIG. 8.—850 μm image of DC 253−1.6 with overlaid polarization vectors rotated by 90° representing the spatial distribution of the magnetic field direction (see § 5.3). Only polarization vectors for which the 850 μm flux exceeds 5 times the standard deviation, $P_l/\sigma P_l > 3$, and $P_l < 5\%$ have been considered. The P axis represents the preferential orientation of the linear polarization, the O axis connects the centers of both sources, and the B axis is oriented perpendicular to the P axis. The angle between the O and P axes amounts to $\varepsilon = 4\overset{\circ}{.}2$ (see § 5.5).

CB 54, DC 253−1.6, and the Serpens cloud core is clearly nonlinear but can be well described by

$$P_l = a_0 + a_1\left[\frac{I}{\max(I)}\right]^{a_2}, \tag{5}$$

where P_l is the degree of linear polarization, I is the measured intensity, and a_0, a_1, and a_2 are constant quantities. For CB 54 we derive

$$a_0 = -1.39 \pm 0.05 ,$$

$$a_1 = 2.16 \pm 0.01 ,$$

and

$$a_2 = -0.64 \pm 0.01 , \tag{6}$$

where P_l is in units of percent. For DC 253−1.6 we get

$$a_0 = -1.31 \pm 0.26 ,$$

$$a_1 = 2.56 \pm 0.14 ,$$

and

$$a_2 = -0.55 \pm 0.02 . \tag{7}$$

Despite the fact that both objects are quite different in their natures (with respect to the number of embedded illuminating sources, the spatial extent, and the magnetic field structure resulting from the polarization pattern), the correlation between the degree of linear polarization and the intensity is strikingly similar. This probably reflects the fact that the radial change of the grain properties and their possible change from one object to another object do not critically influence the coupling of the magnetic field to the

grains. The steep decrease of P_l with increasing I is always found in MHD calculations of self-gravitating cores if it is assumed that grains are not aligned above a critical value of visual extinction (Padoan et al. 2001).

5.5. *Correlation between the Fragmentation Process and the Magnetic Field Direction in DC 253−1.6*

Recent numerical simulations and observations support the hypothesis that the fragmentation of collapsing protostellar cores is the main mechanism for the formation of multiple stellar systems, in particular binary stars (for numerical simulations see, e.g., Bate 2000; Klessen, Burkert, & Bate 1998; Burkert, Bate, & Bodenheimer 1997; Boss 1997; Bonnell & Bate 1994; for evidence from observations see, e.g., Wolf, Stecklum, & Henning 2001; Jensen, Donar, & Mathieu 2000).

Numerical studies predict that the material collapses along the magnetic field lines while the fragmentation occurs in a plane perpendicular to the magnetic field (see, e.g., Fiege & Pudritz 2000a, 2000b). Figure 8 shows the mean magnetic field direction in DC 253−1.6 (represented by the B axis) and the orientation of the binary system (represented by the O axis). The angle between both axes amounts to $90° - \varepsilon = 85\overset{\circ}{.}8$ (corresponding standard deviation of the polarization vectors: $\sigma_{\bar{\gamma}} = 27\overset{\circ}{.}9$; see Table 2), supporting the theoretical prediction.

However, one has to consider that both the magnetic field and the orientation of the two components of DC 253−1.6 are seen only in projection onto the plane of the sky.

6. CONCLUSIONS

For the first time, we obtained submillimeter polarization maps of dense envelopes around the very high density protostellar condensations in Bok globules. We observed the three objects CB 26, CB 54, and DC 253−1.6 and obtained polarization maps at 850 μm. Despite the fact that these Bok globules harbor a different number of embedded sources (CB 26: single source, DC 253−1.6: double core, CB 54: young stellar cluster and unresolved massive core) and show qualitatively different polarization patterns (CB 26, DC 253−1.6: aligned polarization vectors; CB 54: polarization vectors not aligned), we found the following similarities:

1. The degrees of polarization amount to several percent.
2. In the case of CB 54 and DC 253−1.6, where we have a sufficient number of polarization vectors, the degree of polarization decreases toward the globule cores. The functional dependence of this behavior is very similar. This suggests that the optical properties of the grains do not play a key role for the observed polarization decrease, but merely the coupling of the magnetic field to the grains.

The magnetic field strengths we derived from the polarization patterns are well above those of the interstellar medium (see, e.g., Myers et al. 1995). They are similar to those found in molecular cloud cores and protostellar envelopes (see § 5.3).

In the particular case of DC 253−1.6, we found for the first time that this source harbors a double core with a projected distance of about 4×10^3 AU. The fact that the projected orientation of this possible binary system is oriented nearly perpendicular to the magnetic field direction projected onto the plane of the sky supports the hypothesis that the fragmentation process of a collapsing molecular core occurs perpendicular to the magnetic field lines.

A major next step in investigating magnetic field structures in star-forming regions should be the investigation of a larger sample of Bok globules, representing different evolutionary stages to find a solution to the following problems:

1. Are there systematic differences in the structure and strength of the magnetic field in the envelope around low-mass YSOs of different evolutionary stages, located in Bok globules?
2. Do we see evidence for the structure of globules dominated by the magnetic field structure? At which stage of the evolution does the gas decouple from the magnetic fields?

On such a statistical basis, it will be possible to prove basic correlations between the structure and strength of the magnetic field and the dust density distribution that have been investigated theoretically, e.g., by Basu & Mouschovias (1995). The increase in the accuracy of the degree of linear polarization would even allow the derivation of the geometrical shape of the dust grains qualitatively (see Voshchinnikov, Semenov, & Henning 1999) from the combination of the polarization maps with temperature profiles.

The authors wish to acknowledge J. S. Greaves and R. Tilanus for supporting the observations and data reduction. We thank our referee A. Goodman for many helpful comments. This research was supported by DFG grant Ste 605/10 within the program Physics of Star Formation, travel grant He 1935/19-1 of the DFG, and INTAS (Open Call 99/625). R. Launhardt acknowledges financial support through NFS grant AST 99-81546. JCMT is operated by the Joint Astronomy Centre on behalf of the UK Particle Physics and Astronomy Research Council. This publication makes use of data products from the Two Micron All-Sky Survey, which is a joint project of the University of Massachusetts and the Infrared Processing and Analysis Center, funded by the National Aeronautics and Space Administration and the National Science Foundation.

REFERENCES

Arce, H. G., Goodman, A. A., Bastien, P., Manset, N., & Sumner, M. 1998, ApJ, 499, L93
Bastien, P., & Ménard, F. 1988, ApJ, 326, 334
Basu, S. 2000, ApJ, 540, L103
Basu, S., & Mouschovias, T. Ch. 1995, ApJ, 453, 271
Bate, M. R. 2000, MNRAS, 314, 33
Berry, D. S., & Gledhill, T. M. 1999, Starlink User Note 223
Bhatt, H. C., & Jain, S. K. 1992, MNRAS, 257, 57
Bonnell, I. A., & Bate, M. R. 1994, MNRAS, 271, 999
Boss, A. P. 1997, ApJ, 483, 309
Bourke, T. L., Hyland, A. R., & Robinson, G. 1995, MNRAS, 276, 1052
Brand, J., & Blitz, L. 1993, A&A, 275, 67
Burkert, A., Bate, M. R., & Bodenheimer, P. 1997, MNRAS, 289, 497
Casali, M. M. 1995, MNRAS, 277, 1385
Chandrasekhar, S., & Fermi, E. 1953, ApJ, 118, 113
Chrysostomou, A., Hough, J. M., Burton, M. G., & Tamura, M. 1994, MNRAS, 268, 325
Clemens, D. P., & Barvainis, R. 1988, ApJS, 68, 257
Clemens, D. P., & Kraemer, K. E. 1999, AAS Meeting, 194, 47.14
Crutcher, R. M. 1999, ApJ, 520, 706
Davis, C. J., Chrysostomou, A., Matthews, H. E., Jenness, T., & Ray, T. P. 2000, ApJ, 530, L115
Davis, L., & Greenstein, J. L. 1951, ApJ, 114, 206
Dowell, C. D. 1997, ApJ, 487, 237

Draine, B. T., & Weingartner, J. C. 1996, ApJ, 470, 551
———. 1997, ApJ, 480, 633
Efstathiou, A., McCall, A., & Hough, J. H. 1997, MNRAS, 285, 102
Fiedler, R. A., & Mouschovias, T. C. 1993, ApJ, 415, 680
Fiege, J. D., & Pudritz, R. E. 2000a, MNRAS, 311, 105
———. 2000b, ApJ, 534, 291
Fischer, O., Henning, Th., & Yorke, H. W. 1994, A&A, 284, 187
Glenn, J., Walker, C. K., & Young, E. T. 1999, ApJ, 511, 812
Gold, T. 1951, MNRAS, 112, 215
Gonatas, D. P., et al. 1990, ApJ, 357, 132
Goodman, A. A. 1996, in ASP Conf. Ser. 97, Polarimetry of the Interstellar Medium, ed. W. G. Roberge & D. C. B. Whittet (San Francisco: ASP), 325
Goodman, A. A., Jones, T. J., Lada, E. A., & Myers, P. C. 1995, ApJ, 448, 748
———. 1992, ApJ, 399, 108
Greaves, J. S., Holland, W. S., Minchin, N. R., Murray, A. G., & Stevens, J. A. 1999, A&A, 344, 668
Greaves, J. S., Jenness, T., Chrysostomou, A. C., Holland, W. S., & Berry, D. S. 2000, in ASP Conf. Ser. 217, Imaging at Radio through Submillimeter Wavelengths, ed. J. G. Mangum & S. J. E. Radford (San Francisco: ASP), 150
Greaves, J. S., Murray, A. G., & Holland, W. S. 1994, A&A, 284, L19
Hartley, M., Tritton, S. B., Manchester, R. N., Smith, R. M., & Goss, W. M. 1986, A&AS, 63, 27
Henning, Th., & Launhardt, R. 1998, A&A, 338, 223
Hildebrand, R. H. 1996, in ASP Conf. Ser. 97, Polarimetry of the Interstellar Medium, ed. W. G. Roberge & D. C. B. Whittet (San Francisco: ASP), 254
Hildebrand, R. H., Davidson, J. A., Dotson, J., Figer, D. F., Novak, G., Platt, S. R., & Tao, L. 1993, ApJ, 417, 565
Hildebrand, R. H., Dotson, J. L., Dowell, C. D., Schleuning, D. A., & Vaillancourt, J. E. 1999, ApJ, 516, 834
Hildebrand, R. H., & Dragovan, M. 1995, ApJ, 450, 663
Hildebrand, R. H., Gonatas, D. P., Platt, S. R., Wu, X. D., Davidson, J. A., Werner, M. W., Novak, G., & Morris, M. 1990, ApJ, 362, 114
Hodapp, K.-W., & Ladd, E. F. 1995, ApJ, 453, 715
Holland, W. S., et al. 1999, MNRAS, 303, 659
Itoh, Y., Chrysostomou, A., Burton, M., Hough, J. H., & Tamura, M. 1999, MNRAS, 304, 406
Jenness, T., & Lightfoot, J. F. 1998, in ASP Conf. Ser. 145, Astronomical Data Analysis Software and Systems VII, ed. R. Albrecht, R. N. Hook, & H. A. Bushouse (San Francisco: ASP), 216
Jenness, T., Lightfoot, J. F., & Holland, W. S. 1998, Proc. SPIE, 3357, 548
Jensen, E., Donar, A. X., & Mathieu, R. D. 2000, in Birth and Evolution of Binary Stars, ed. B. Reipurth & H. Zinnecker (Potsdam: Astrophys. Inst. Potsdam)
Jones, T. J., Klebe, D., & Dickey, J. M. 1992, ApJ, 389, 602
Klessen, R. S., Burkert, A., & Bate, M. R. 1998, ApJ, 501, L205
Knude, J., Jønch-Sørensen, H., & Nielsen, A. S. 1999, A&A, 350, 985
Larson, K. A., Whittet, D. C. B., & Hough, J. H. 1996, ApJ, 472, 755
Launhardt, R. 1996, Ph.D. thesis, Univ. Jena
Launhardt, R., Evans, N. J., Wang, Y., Clemens, D. P., Henning, Th., & Yun, J. L. 1998, ApJS, 119, 59
Launhardt, R., & Henning, Th. 1997, A&A, 326, 329
Launhardt, R., Sargent, A. I., Henning, Th., Zylka, R., & Zinnecker, H. 2001a, in Birth and Evolution of Binary Stars, Poster Proc. of IAU Symp. 200, ed. B. Reipurth & H. Zinnecker (Potsdam: Astrophys. Inst. Potsdam), 103
Launhardt, R., Sargent, A. I., & Zinnecker, H. 2001b, ApJ, submitted
Launhardt, R., Ward-Thompson, D., & Henning, Th. 1997, MNRAS, 288, L45
Lazarian, A. 1995, ApJ, 451, 660
Lazarian, A., Goodman, A. A., & Myers, P. C. 1997, ApJ, 490, 273
Levin, S. M., Langer, W. D., Velusamy, T., & Kuiper, T. B. H. 2001, ApJ, in press
Lynds, B. T. 1962, ApJS, 7, 1
———. 1965, ApJS, 12, 163
Matthews, B. C., & Wilson, C. D. 2000, ApJ, 531, 868
McKee, C. F. 1999, in The Origin of Stars and Planetary Systems, ed. C. J. Lada & N. D. Kylafis (Dordrecht: Kluwer), 29
Minchin, N. R., Bonifaćio, V. H. R., & Murray, A. G. 1996, A&A, 315, L5
Minchin, N. R., & Murray, A. G. 1994, A&A, 286, 579
Morris, M., Davidson, J. A., Werner, M., Dotson, J., Figer, D. F., Hildebrand, R., Novak, G., & Platt, S. 1992, ApJ, 399, L63
Mouschovias, T. Ch., & Ciolek, G. E. 1999, in The Origin of Stars and Planetary Systems, ed. C. J. Lada & N. D. Kylafis (Dordrecht: Kluwer), 305
Murray, A. G., Nartallo, R., Haynes, C. V., Gannaway, F., & Ade, P. A. R. 1997, in Proc. ESA Symp., The Far Infrared and Submillimetre Universe, ed. A. Wilson (Noordwijk: ESA), 405
Myers, P. C., Goodman, A. A., Gusten, R., & Heiles, C. 1995, ApJ, 442, 177
Novak, G., Dotson, J. L., Dowell, C. D., Goldsmith, P. F., Hildebrand, R. H., Platt, S. R., & Schleuning, D. A. 1997, ApJ, 487, 320
Ostriker, E. C., Stone, J. M., & Gammie, C. F. 2001, ApJ, 546, 980
Padoan, P., Goodman, A., Draine, B., Juvela, M., Nordlund, Å., & Rögnvaldsson, Ö. 2001, ApJ, 559, 1005
Purcell, E. M. 1975, in The Dusty Universe, ed. F. L. Whipple, G. B. Field, & A. G. W. Cameron (New York: Neale Watson), 155
———. 1979, ApJ, 231, 404
Roberts, D. A., Dickel, H. R., & Goss, W. M. 1997, ApJ, 476, 209
Shu, F., Adams, F., & Lizano, S. 1987, ARA&A, 25, 23
Shu, F. H., Allen, A., Shang, H., Ostriker, E. C., & Li, Z. Y. 1999, in The Origin of Stars and Planetary Systems, ed. C. J. Lada & N. D. Kylafis (Dordrecht: Kluwer), 193
Voshchinnikov, N. V., Semenov, D. A., & Henning, Th. 1999, A&A, 349, L25
Wang, Y., Evans, N. J., II, Zhou, S., & Clemens, D. P. 1995, ApJ, 454, 217
Ward-Thompson, D., Kirk, J. M., Crutcher, R. M., Greaves, J. S., Holland, W. S., & André, P. 2000, ApJ, 537, L135
Weintraub, D. A., Goodman, A. A., & Akeson, R. L. 2000, in Protostars and Planets IV, ed. V. Mannings, A. P. Boss, & S. S. Russell (Tucson: Univ. Arizona Press), 247
Whittet, D. C. B., Gerakines, P. A., Carkner, A. L., Hough, J. H., Martin, P. G., Prusti, T., & Kilkenny, D. 1994, MNRAS, 268, 1
Wolf, S., Stecklum, B., & Henning, Th. 2001, in ASP Conf. Ser., The Formation of Binary Stars, ed. H. Zinnecker & B. Mathieu (San Francisco: ASP), in press
Wood, K. 1996, AAS Meeting, 189, 67.08
———. 1997, ApJ, 477, L25
Yun, J. L. 1996, AJ, 111, 930
Yun, J. L., & Clemens, D. P. 1994, ApJS, 92, 145
Zealey, W. J., Ninkov, Z., Rice, E., Hartley, M., & Tritton, S. B. 1983, ApJ, 23, L119
Zweibel, E. G. 1990, ApJ, 362, 545